

[3]

## Simple 2-D models for melt extraction at mid-ocean ridges and island arcs

Marc Spiegelman and Dan McKenzie

*Department of Earth Sciences, University of Cambridge, Downing Street, Cambridge, CB2 3EQ (England)*

Received August 15, 1986; revised version accepted February 1, 1987

A general set of 2-D equations for the conservation of mass and momentum of a two-phase system of melt in a deformable matrix is used to derive analytic solutions for the corner flow of a constant porosity melt-saturated porous medium. This solution is used to model the melt extraction processes at mid-ocean ridges and island arcs. The models indicate that flow of melt is controlled by pressure gradients induced by the Laplacian of the matrix velocity field and by the dimensionless percolation velocity which measures the relative contributions of buoyancy-driven flow to advection by the matrix. The models can account for many features of ridge and arc volcanism. Matrix corner flow at ridges causes melt to be drawn to the ridge axis enabling the extraction of small melt fractions from a wide melting zone while showing a narrow zone of volcanism at the surface. At subduction zones melts do not percolate vertically but are drawn to the junction of the upper plate and subducting slab by corner flow in the mantle wedge. For subduction zones, if the dimensionless percolation velocity is below a critical value, slab-derived fluids will be carried down by the matrix and cannot interact with the mantle wedge. The geochemistry of island arcs will be controlled by the geometry of melt streamlines. This model is consistent with geophysical and geochemical data from the Aleutian arc.

### 1. Introduction

It is generally accepted that partial melting with subsequent separation from the solid residue is the primary process governing the production of melt at oceanic spreading centers and subduction zones, yet little is actually understood of the physical processes involved. As estimates of global magmatism indicate that oceanic magmatism accounts for approximately 75% of global output [1] it is important that work be done to quantify these processes.

Until recently, however, this has been difficult for lack of a comprehensive system of equations governing conservation of mass, momentum and energy for a two-phase system that takes into account the deformation of the solid, crystalline matrix. This has been remedied by several workers [2–4] who have proposed several similar sets of equations. Here we will use McKenzie's formulation and notation.

As these equations are rather complicated, it is necessary to investigate their properties systematically by looking at simple problems. The simplest subset of problems are one dimensional and several workers have investigated 1-D compaction of a

melt-saturated medium [3,5], melting and compaction for simple 1-D upwelling models with ad hoc melting functions [6,7] and the existence and stability of 1-D porosity waves and solitons [4,5,8].

The purpose of this paper is to carry this work into two dimensions by using a general set of 2-D equations for the conservation of mass and momentum to derive analytic solutions to the simplest case of corner flow of a constant porosity melt-saturated porous medium. These models are then used to illustrate the melt extraction processes which may occur at spreading centers and subduction zones.

### 2. Governing equations

The general governing equations for the conservation of mass and momentum of a low viscosity "melt" or "fluid" phase in a deformable "matrix" can be written [3]:

$$\frac{\partial}{\partial t}(\rho_f \phi) + \nabla \cdot (\rho_f \phi \mathbf{v}) = \Gamma \quad (1)$$

$$\frac{\partial}{\partial t}[\rho_s(1 - \phi)] + \nabla \cdot [\rho_s(1 - \phi)\mathbf{V}] = -\Gamma \quad (2)$$

$$\mathbf{v} - \mathbf{V} = \frac{-k_\phi}{\phi\mu} \nabla \mathcal{P} \quad (3)$$

$$\nabla \mathcal{P} = \eta \nabla^2 V + (\zeta + \eta/3) \nabla(\nabla \cdot V) + (1 - \phi) \Delta \rho g \hat{k} \quad (4)$$

$$k_\phi \sim a^2 \phi^n / c \quad (5)$$

where  $\rho_f$  is the density of the melt,  $\phi$  is the volume fraction occupied by the melt or porosity,  $v$  is the melt velocity,  $\Gamma$  is the "melting function" which gives the rate of mass transfer from matrix

TABLE I

Notation

Variable	Meaning	Value used	Dimension
$a$	grain size	$10^{-3}$	m
$c$	constant in permeability	1000	none
$d$	thickness of oceanic lithosphere		km
$g$	acceleration due to gravity	9.81	$\text{m s}^{-2}$
$h$	thickness of oceanic crust		km
$k_\phi$	permeability		$\text{m}^2$
$k_0$	$= a^2 \phi_0^3 / c$ permeability at porosity $\phi_0$		$\text{m}^2$
$l$	thickness of melting zone	30–60	km
$L$	$= [\eta U_0 / \Delta \rho g]^{1/2}$ length scale		m
$L_R$	length scale for ridge model		m
$L_T$	length scale for trench model		m
$p$	degree of partial melting	0.1–0.3	none
$\mathcal{P}$	piezometric pressure		Pa
$\mathcal{P}_R$	dimensionless piezometric pressure, ridge model		none
$\mathcal{P}_T$	dimensionless piezometric pressure, trench model		none
$r$	polar coordinate (distance from corner)		m
$r'$	$= r/L$ dimensionless polar coordinate		none
$t$	time		s
$U_0$	characteristic velocity: half spreading rate, ridge model subduction rate, trench model	$10^{-10}$ – $10^{-9}$	$\text{m s}^{-1}$
$V$	matrix velocity		$\text{m s}^{-1}$
$v$	melt velocity		$\text{m s}^{-1}$
$V', v'$	$= V, v/U_0$ dimensionless velocities		none
$\Delta v$	specific volume change on melting		$\text{m}^3 \text{kg}^{-1}$
$w_0$	$= k_0(1 - \phi_0) \Delta \rho g / \phi_0 \mu$ percolation velocity		$\text{m s}^{-1}$
$x$	horizontal cartesian coordinate		m
$z$	vertical cartesian coordinate		m
$x', z'$	$= x, z/L$ dimensionless cartesian coordinates		none
$\alpha$	wedge angle (ridge model)	$(10-40^\circ)$	none
$\beta$	angle of subduction (trench model)	$(30-80^\circ)$	none
$\Gamma$	$= D_v M / D t$ (McKenzie [3]) melting function		$\text{kg m}^{-3} \text{s}^{-1}$
$\zeta$	matrix bulk viscosity	$10^{18}$ – $10^{21}$	Pa s
$\eta$	matrix shear viscosity	$10^{18}$ – $10^{21}$	Pa s
$\theta$	polar coordinate		none
$\kappa$	thermal diffusivity of lithosphere	$10^{-6}$	$\text{m}^2 \text{s}^{-1}$
$\mu$	melt shear viscosity	1	Pa s
$\rho_c$	mean density of oceanic crust	2800	$\text{kg m}^{-3}$
$\rho_f$	density of melt	2800	$\text{kg m}^{-3}$
$\rho_s$	density of matrix	3300	$\text{kg m}^{-3}$
$\Delta \rho$	$= \rho_s - \rho_f$	500	$\text{kg m}^{-3}$
$\phi$	porosity		none
$\phi_0$	characteristic porosity (constant)	0.006–0.04	none
$\psi$	stream function		$\text{m}^2 \text{s}^{-1}$
$\psi_R^f$	dimensionless melt stream function ridge model		none
$\psi_T^f$	dimensionless melt stream function trench model		none
$\psi_R^s$	dimensionless matrix stream function ridge model		none
$\psi_T^s$	dimensionless matrix stream function trench model		none

to melt in a frame fixed to the matrix ( $\Gamma = D_V M / Dt$  in McKenzie [3]).  $\rho_s$  is the density of the solid matrix,  $V$  is the matrix velocity,  $k_\phi$  is the permeability,  $\mathcal{P}$  is the “piezometric pressure” or the pressure in excess of “hydrostatic pressure” ( $\mathcal{P} = P - \rho_f g z$ ),  $\Delta\rho = \rho_s - \rho_f$  and  $\hat{k}$  is the unit vector in the  $z$  direction with  $z$  increasing downwards. Equation (5) gives the permeability as a non-linear function of the grain size  $a$ , porosity and a dimensionless coefficient,  $c$ . Estimates and explanations of parameters are given in Table 1.

The first two equations govern the conservation of mass for the melt and matrix respectively. Equation (3) is Darcy’s Law which states that the separation velocity of melt from matrix depends on the permeability and lies along gradients of the piezometric pressure. Equation (4) shows that the piezometric pressure has three contributing factors. The first term on the right-hand side is the pressure gradient due to volume conserving shear deformation of the matrix. It should be noted that only deformation with non-zero  $\nabla^2 V$  will cause changes in the pressure. Uniform simple shear or pure shear will have no effect on the melt flow as they have constant first derivatives. The second term in equation (4) is the gradient due to volume changes of the matrix on expansion and compaction and the third term is the gradient due to the differential buoyancy between melt and matrix.

It is important to note that in one dimension there is no distinction between shear deformation and compaction. In two and three dimensions, however, the difference is quite significant for even in the simplest case described below, where compaction is neglected, the shear deformation controls the geometry of melt extraction.

### 3. Governing equations in 2-D, constant density

If  $\rho_f$  and  $\rho_s$  are constant, then in two dimensions equations (1) to (4) represent 6 equations in 7 unknowns. If the melting function,  $\Gamma$ , is known then equations (1) to (4) can be solved for  $\phi$ ,  $\mathcal{P}$  and 2 components each of  $v$  and  $V$ . In two dimensions, however, the problem can be reduced to solving only three equations for the porosity and matrix velocity subject to appropriate boundary conditions. Once  $\phi$  and  $V$  are known, the piezometric pressure, permeability, and therefore the melt velocity are completely determined

by equations (3) to (5). These general 2-D equations are given in Appendix A and are rather complicated. We have not made much progress in obtaining analytical solutions and further work will require careful numerical investigation. However, if porosity is constant and melting neglected, the problem becomes surprisingly simple and analytical solutions can be found that demonstrate much of the significant physics of melt extraction. The analytical solutions can also account for many of the features of volcanism at mid-ocean ridges and subduction zones.

### 4. Simple corner flow models: constant porosity, no melting

Corner flow of a viscous incompressible fluid has often been used to model the flow of the mantle near spreading centers and subduction zones [9–11]. As these regions of the mantle are probably partially molten a better approximation is to examine the two phase corner flow of a melt saturated, deformable porous medium. The solid matrix behaves like the viscous fluid in the previous models but the melt in the pores obeys Darcy’s law and flows in response to gradients in the piezometric pressure. In the simplest model the porosity is constant and melting is ignored. This necessarily rules out compaction. Mathematically,  $\phi = \phi_0$ ,  $\Gamma = 0$  implies that:

$$\nabla \cdot V = \nabla \cdot v = 0 \quad (6)$$

from equations (1) and (2), and therefore  $V$  and  $v$  can be written in potential form in terms of scalar stream functions:

$$\begin{aligned} V &= \nabla \times (\psi^s \hat{j}) \\ v &= \nabla \times (\psi^f \hat{j}) \end{aligned} \quad (7)$$

where  $\hat{j}$  is the unit vector perpendicular to the  $x$ ,  $z$  plane. As is shown in Appendix A, the problem then reduces to simply solving the biharmonic equation:

$$\nabla^4 \psi^s = 0 \quad (8)$$

for the matrix stream function subject to appropriate boundary conditions.

Batchelor [12] gives a similarity solution to the biharmonic equation with corner flow boundary conditions. He shows that this problem can be

solved by inspection in polar coordinates with:

$$\mathcal{V} = \frac{1}{r} \frac{\partial \psi^s}{\partial \theta} \hat{r} - \frac{\partial \psi^s}{\partial r} \hat{\theta} \quad (9)$$

$$\psi^s = r U_0 f(\theta) \quad (10a)$$

and:

$$f(\theta) = C_1 \sin \theta + C_2 \theta \sin \theta + C_3 \cos \theta + C_4 \theta \cos \theta \quad (10b)$$

where  $U_0$  is a characteristic velocity (i.e. the half-spreading rate for the ridge model and the subduction rate for the trench model),  $r$  is the distance measured from the corner,  $\theta$  is the angle measured from an arbitrary zero axis and  $C_{1-4}$  are constants adjusted to match the two components of the velocity on each of two straight boundaries. Given the matrix stream function, the piezometric pressure and the melt stream function are completely determined and can be written:

$$\mathcal{P} = \frac{-\eta U_0}{r} \left( \frac{d^3 f}{d\theta^3} + \frac{df}{d\theta} \right) + z(r, \theta)(1 - \phi_0) \Delta \rho g \quad (11)$$

$$\psi^f = \frac{-k_0}{\phi_0 \mu} \left[ \frac{\eta U_0}{r} \left( \frac{d^2 f}{d\theta^2} + f \right) + x(r, \theta)(1 - \phi_0) \Delta \rho g \right] + \psi^s \quad (12)$$

where in this case, the permeability is given by the Blake-Kozeny-Carman equation [3,13]:

$$k_0 = \frac{a^2 \phi_0^3}{c} \quad (13)$$

and  $x$  and  $z$  are standard cartesian coordinates.

Dimensional analysis shows that the piezometric pressure is governed by a single length scale:

$$L = \left[ \frac{\eta U_0}{(1 - \phi_0) \Delta \rho g} \right]^{1/2} \quad (14)$$

which is the length scale governing extraction of melt by shear in the matrix. This expression suggests a useful non-dimensionalization which reveals the essential physics. Let:

$$(x, z, r) = (x', z', r') L \quad (15)$$

$$(\psi^s, \psi^f) = (\psi^s, \psi^f)' U_0 L$$

$$\mathcal{P} = \mathcal{P}' (1 - \phi_0) \Delta \rho g L$$

Substituting and dropping primes yields:

$$\psi^s = r f(\theta) \quad (16)$$

$$\mathcal{P} = \frac{-1}{r} \left( \frac{d^3 f}{d\theta^3} + \frac{df}{d\theta} \right) + z(r, \theta) \quad (17)$$

$$\psi^f = \frac{-w_0}{U_0} \left[ \frac{1}{r} \left( \frac{d^2 f}{d\theta^2} + f \right) + x(r, \theta) \right] + \psi^s \quad (18)$$

where:

$$w_0 = \frac{k_0 (1 - \phi_0) \Delta \rho g}{\phi_0 \mu} \quad (19)$$

is the ‘‘percolation velocity’’, that is, the separation velocity between the melt and the matrix given by Darcy’s law in the absence of matrix deformation. Note that  $w_0$  depends on the square of the porosity. Equation (18) shows that the melt will follow the matrix stream lines only if the dimensionless percolation velocity,  $w_0/U_0 = 0$ , and that contrary to most simple petrological models, it will percolate vertically only in the absence of matrix deformation.

## 5. Ridge model: solution and results

Boundary conditions for the ridge model are shown in Fig. 1a. The wedge geometry is due to several workers [10,11] and is used to approximate the thickening lithosphere near a ridge crest due to cooling. Polar coordinates are defined by:

$$\begin{aligned} x &= r \sin \theta \\ z &= r \cos \theta \end{aligned} \quad (20)$$

with the  $\theta = 0$  being the axis of symmetry. The dimensionless boundary conditions for this geometry are

$$\begin{aligned} &\text{at } \theta = (\pi/2 - \alpha): \\ &\frac{1}{r} \frac{\partial \psi_R^s}{\partial \theta} = \cos \alpha \quad \frac{\partial \psi_R^s}{\partial r} = -\sin \alpha \\ &\text{at } \theta = -(\pi/2 - \alpha): \\ &\frac{1}{r} \frac{\partial \psi_R^s}{\partial \theta} = \cos \alpha \quad \frac{\partial \psi_R^s}{\partial r} = \sin \alpha \end{aligned} \quad (21)$$

where  $\alpha$  is the wedge angle. The dimensionless matrix stream function is given by equations (10) and (16) as:

$$\psi_R^s = r(A \sin \theta - B \theta \cos \theta) \quad (22a)$$

where:

$$\begin{aligned} A &= \frac{2 \sin^2 \alpha}{\pi - 2\alpha - \sin 2\alpha} \\ B &= \frac{2}{\pi - 2\alpha - \sin 2\alpha} \end{aligned} \quad (22b)$$

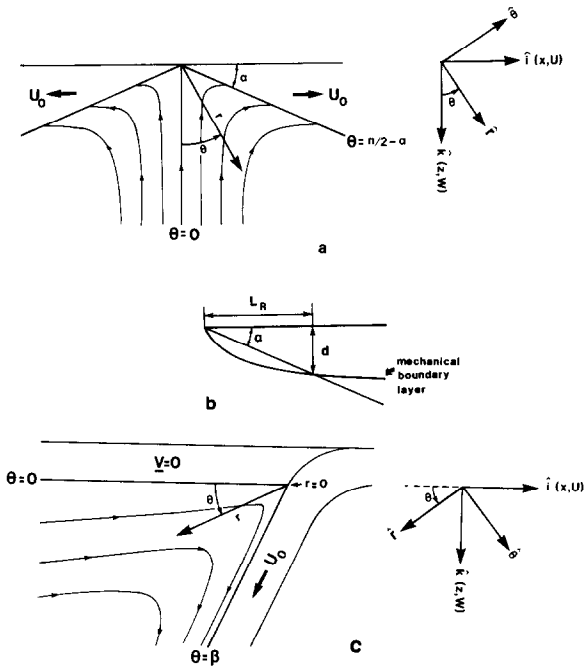


Fig. 1. (a) Boundary conditions for corner flow ridge model showing matrix streamlines and coordinate systems. (b) Definition of wedge angle  $\alpha$ .  $L_R$  is the characteristic length scale for the ridge model,  $d$  is the depth to the base of the mechanical boundary layer (equation (B1)). (c) Boundary conditions for corner flow trench model showing matrix streamlines and coordinate systems.  $\theta$  is defined differently from 1a.

The dimensionless piezometric pressure and melt stream function are then:

$$\mathcal{P}_R = \left( \frac{-2B}{r} + r \right) \cos \theta \quad (23)$$

$$\psi_R^f = \frac{-w_0}{U_0} \left( \frac{2B}{r} + r \right) \sin \theta + \psi_R^s \quad (24)$$

The principal features of this simple model can be easily seen in Figs. 2 and 3 which show melt and matrix streamlines for reasonable combinations of spreading rate, matrix viscosity and porosity. Given  $U_0$  and  $\eta$ , the wedge angle  $\alpha$  is approximated using an argument from Skilbeck [10] (Appendix B).

The most noticeable aspect of this model is the convergence of melt streamlines towards the ridge axis in contrast to the diverging matrix flow. This focussing effect is due to the first term in the piezometric pressure and arises from the pressure gradient due to shear in the matrix. Equation (23) shows that this effect decays away from the corner

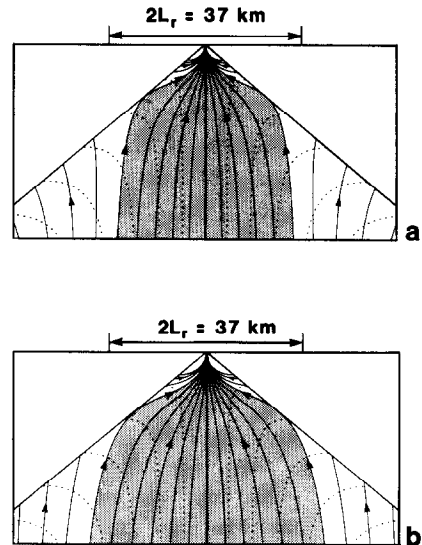


Fig. 2. Melt streamlines (solid) and matrix streamlines (dashed) for slow-spreading ridges,  $U_0 = 1$  cm yr $^{-1}$  ( $\alpha = 40^\circ$ ), matrix shear viscosity,  $\eta = 10^{21}$  Pa s. Stippled region is the melt extraction zone containing all melt streamlines connecting the ridge axis to depth.  $h$  is the crustal thickness produced by the extraction zone. All figures are true scale. (a) Low porosity,  $w_0/U_0 = 1.56$  ( $\phi_0 = 1.0\%$ ),  $h = 0.5$  km. (b) High porosity sufficient to produce  $\sim 6$  km of crust,  $w_0/U_0 = 9.12$  ( $\phi_0 = 2.4\%$ ),  $h = 6.5$  km.

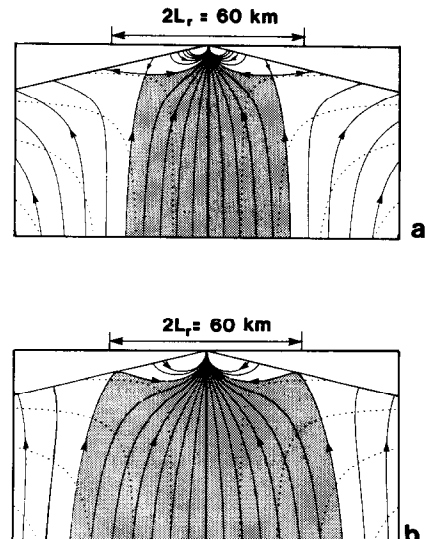


Fig. 3. Melt and matrix streamlines for fast spreading ridges.  $U_0 = 7.5$  cm yr $^{-1}$  ( $\alpha = 13^\circ$ ),  $\eta = 10^{21}$  Pa s. (a) Low porosity, showing saddlepoint in the melt stream function,  $w_0/U_0 = 0.47$  ( $\phi_0 = 1.5\%$ ),  $h = 0.5$  km. (b) High porosity, sufficient to produce  $\sim 6$  km of crust,  $w_0/U_0 = 2.77$  ( $\phi_0 = 3.6\%$ ),  $h = 6.1$  km.

as  $1/r$  with a characteristic length scale of  $L_R = L(2B)^{1/2}$ . Because of this decay not all melt at depth is extracted at the ridge axis. In all cases there is a region of melt extraction, shown in stipple, in which the melt streamlines from depth pass through the axis. Outside this region, melt is incorporated into the lithospheric wedge and may solidify or generate off-axis volcanism.

The absolute value of the bounding streamlines depends only on the dimensionless percolation velocity,  $w_0/U_0$ , and the wedge angle  $\alpha$ . If  $w_0/U_0$  is small (e.g. porosity is small), then equation (24) shows that the effect of the singularity will be diminished, advection of melt by the matrix will be significant and the melt streamlines will approximately follow those of the matrix (if  $w_0/U_0 = 0$ , they will be identical). In this case there will be a point where the advection of melt by the matrix is balanced by the pressure gradient towards the singularity and the melt velocity will be zero in a frame fixed to the ridge axis. Mathematically this corresponds to a saddlepoint in the stream function and the bounding streamlines will be the ones that pass through this point. This saddlepoint is apparent in Fig. 3a, and is obtained numerically (Appendix B). As  $w_0/U_0 \rightarrow 0$  the saddlepoint moves towards the origin and as  $w_0/U_0 \rightarrow \infty$  the position of the saddlepoint tends to  $r = L_R$ ,  $\theta = \pm\pi/2$ . If the computed saddlepoint lies outside the boundaries of the wedge, then the bounding streamline will be the one that is tangent to the boundary. This situation is illustrated in Figs. 2a, b and 3b.

The dimensional mass flux of melt per unit length of ridge that can be extracted from this region is:

$$\frac{dM_R}{dt} = 2\rho_f \phi_0 U_0 L |\psi_{R \text{ bound}}^f| \quad (25)$$

where  $\psi_{R \text{ bound}}^f$  is the dimensionless value of the bounding streamline. A more useful measurement, however, is the crustal thickness produced by this melt flux which is simply the area flux divided by the spreading rate or:

$$h = \frac{\rho_f}{\rho_c} \phi_0 L |\psi_{R \text{ bound}}^f| \quad (26)$$

where  $\rho_c$  is the average density of oceanic crust.

The crustal thickness is perhaps the most important result produced by this model and can be

used to put constraints on the values of the various parameters. Dimensional analysis shows that the crustal thickness behaves as:

$$h \propto \phi_c L \frac{w_0}{U_0} \sim \frac{a^2 \phi_0^3}{\mu} \left[ \frac{\eta \Delta \rho g}{U_0} \right]^{1/2} \quad (27)$$

and therefore depends primarily on the mean porosity and the shear viscosity of the mantle. The simple model also predicts that, all else being equal, faster spreading ridges should produce thinner crust than slow ridges. The discussion will deal with the probable ranges of  $\phi$  and  $\eta$ , their implications for the mechanics of mid-ocean ridges, and a possible explanation for the apparent independence of oceanic crustal thickness from spreading rate.

## 6. Subduction zone model: solution and results

Boundary conditions for the subduction model are shown in Fig. 1c. In this case it is mathematically convenient to define polar coordinates in a slightly different way than the ridge model by:

$$\begin{aligned} x &= -r \cos \theta \\ z &= r \sin \theta \end{aligned} \quad (28)$$

The dimensionless boundary conditions are

$$\begin{aligned} \text{at } \theta = 0: \\ \frac{1}{r} \frac{\partial \psi_T^s}{\partial \theta} = 0 \quad \frac{\partial \psi_T^s}{\partial r} = 0 \\ \text{at } \theta = \beta: \\ \frac{1}{r} \frac{\partial \psi_T^s}{\partial \theta} = 1 \quad \frac{\partial \psi_T^s}{\partial r} = 0 \end{aligned} \quad (29)$$

where  $\beta$  is the angle of subduction. The dimensionless matrix stream function is given by equations (10) and (16) as:

$$\psi_T^s = r [C(\sin \theta - \theta \cos \theta) + D\theta \sin \theta] \quad (30a)$$

where:

$$\begin{aligned} C &= \frac{\beta \sin \beta}{\beta^2 - \sin^2 \beta} \\ D &= \frac{\beta \cos \beta - \sin \beta}{\beta^2 - \sin^2 \beta} \quad (D < 0) \end{aligned} \quad (30b)$$

The dimensionless piezometric pressure and melt stream function are then:

$$\mathcal{P}_T = \frac{-2}{r} (C \cos \theta - D \sin \theta) + r \sin \theta \quad (31)$$

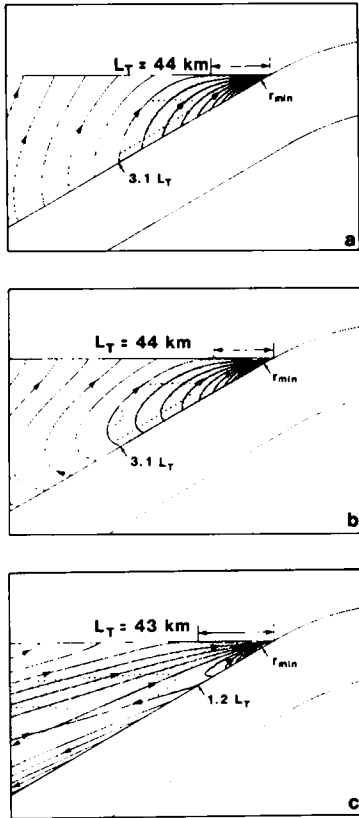


Fig. 4. Melt (solid) and matrix (dashed) streamlines for shallow angle of subduction,  $\beta = 30^\circ$ . Subduction rate,  $U_0 = 7.5 \text{ cm yr}^{-1}$ ,  $\eta = 10^{21} \text{ Pa s}$ . Stippled region is the melt extraction zone containing all streamlines from depth that connect to the wedge corner. The melt flux is calculated through a circular arc at  $r_{\min} = 2^{1/2} L/4$ . Also shown is the length of slab sampled at the primary arc. The mantle wedge is true scale but the slab thickness is schematic for illustration only. (a) High porosity,  $\phi_0 = 3.0\%$ , wedge corner is entirely connected to slab.  $w_0/U_0 = 1.91$ , flux =  $2.4 \times 10^{-3} \text{ km}^2 \text{ yr}^{-1}$ . (b) Medium porosity,  $\phi_0 = 1.5\%$ . Lower permeability causes streamlines to “bulge” as melt flow is more affected by downwards matrix flow. The streamlines, however, begin and end in the same positions as (a).  $w_0/U_0 = 0.47$ , flux =  $2.9 \times 10^{-4} \text{ km}^2 \text{ yr}^{-1}$ . (c) Low porosity,  $\phi_0 = 0.6\%$ .  $w_0/U_0 = 0.07$  is less than the critical value and a saddlepoint exists in the melt stream function causing the slab to partially disconnect from the corner. The length of slab sampled at the arc is less than in (a) and (b). Flux =  $1.8 \times 10^{-5} \text{ km}^2 \text{ yr}^{-1}$ , slab fraction = 79%.

$$\psi_1^f = \frac{-w_0}{U_0} \left[ \frac{2}{r} (C \sin \theta + D \cos \theta) - r \cos \theta \right] + \psi_T^s \quad (32)$$

The principal features of the trench model can be seen clearly in Figs. 4 and 5. As in the ridge

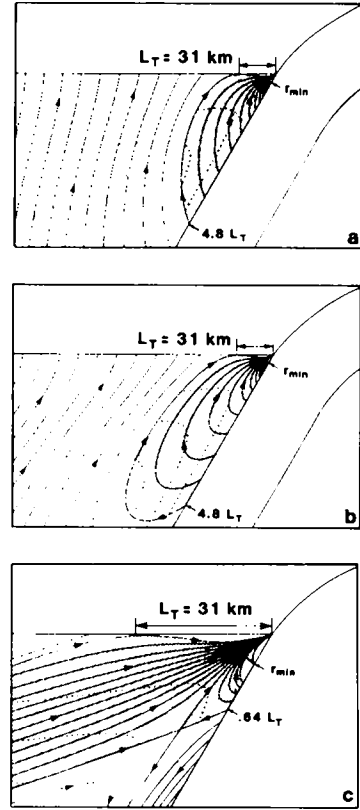


Fig. 5. As for Fig. 4 with a steeper subduction angle,  $\beta = 60^\circ$ ,  $U_0 = 7.5 \text{ cm yr}^{-1}$ ,  $\eta = 10^{21} \text{ Pa s}$ . (a) High porosity,  $\phi_0 = 3.0\%$ .  $w_0/U_0 = 1.91$ , flux =  $1.2 \times 10^{-3} \text{ km}^2 \text{ yr}^{-1}$ . (b) Medium porosity,  $\phi_0 = 1.5\%$ . The effect of downward advection by the matrix is more pronounced for larger  $\beta$ .  $w_0/U_0 = 0.47$ , flux =  $1.5 \times 10^{-4} \text{ km}^2 \text{ yr}^{-1}$ . (c) Low porosity,  $\phi_0 = 0.6\%$ . Subcritical  $w_0/U_0 = 0.07$ , shows saddlepoint. Back arc is entirely disconnected from the slab. Flux =  $9.4 \times 10^{-6} \text{ km}^2 \text{ yr}^{-1}$ , slab fraction = 50%.

model, melt that lies in the extraction zone, shown in stipple, is drawn to the wedge corner ( $r = 0$ ) by a singularity in the piezometric pressure at the corner. Any melt outside this region follows the streamlines until it intersects the lower boundary of the plate above the sinking slab ( $\theta = 0$ ) and then percolates vertically, either to the surface or until it becomes incorporated into the upper plate.

The surface expression of this behaviour will be marked by a narrow region of primary magmatism directly above the wedge corner followed by a narrow quiet zone of width  $L_T = L(-2D)^{1/2}$ , where the melt moves downwards and volcanism should be absent, succeeded by a broad region of diffuse magmatism. If the region of primary

magmatism above  $r = 0$  represents the volcanic arc then it is important to note that the melt extracted at island arcs is not representative of the mantle directly beneath the arc but of a much larger region of melting. The behaviour of this extraction zone is surprisingly complex given the simplicity of the model. The shape of the extraction zone is controlled by the angle of subduction and the dimensionless percolation velocity. The size, of course, is controlled by  $L$ , the only length scale in this problem.

Analysis shows (Appendix B) that the points at which the bounding streamline intersects the upper plate ( $\theta = 0$ ,  $r = L_T$ ) and the subducting slab ( $\theta = \beta$ ,  $r = r_\beta$ ) depend only on the angle of subduction and  $L$ ; therefore, the width of the quiet zone and the maximum length of slab that can be sampled by the arc magmatism are independent of porosity. This result can be seen by comparing Fig. 4a to 4b and 5a to 5b which show similar geometries but different porosities. Though the ends of the bounding streamline are fixed by  $\beta$  and  $L$ , the path is controlled by  $w_0/U_0$  and therefore by the porosity. If  $w_0/U_0$  is large, flow of melt is dominated by buoyancy and the draw of the singularity. Therefore the melt will tend to flow vertically then towards the wedge corner (Figs. 4a, 5a). However, as  $w_0/U_0$  becomes smaller, upward percolation is resisted by downwards matrix flow and the melt will flow out sideways away from the slab until it can percolate upwards. This causes the bounding streamline to bulge outwards (Figs. 4b, 5b).

This "bulging" will increase with decreasing  $w_0/U_0$  until a critical value of  $w_0/U_0$  is reached, at which point the streamlines separate and the melt streamlines from the slab become partially disconnected from those in the overlying mantle wedge. Analysis shows that this critical value depends only on the angle of subduction (Appendix B). This relationship is shown in Fig. 6.

Therefore, for a given subduction angle, if  $w_0/U_0$  is greater than the critical value all streamlines passing through the wedge corner, and therefore to the arc, will be connected to the subducting slab (Figs. 4a, b; 5a, b). However, if  $w_0/U_0$  is less than critical then a saddle point in the melt stream function exists where the draw of the singularity balances the drag of the matrix and the last streamline that connects the subducting slab

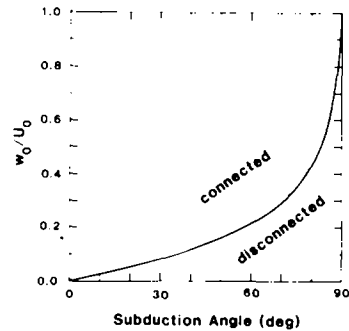


Fig. 6. Solid line is the critical dimensionless percolation velocity ( $w_0/U_0$ ) as a function of subduction angle. For  $w_0/U_0$  greater than critical, the slab is entirely connected to the surface. The slab becomes partially disconnected for  $w_0/U_0$  less than critical.

to the arc will be the streamline that passes through the saddlepoint (Figs. 4c, 5c). Any melt from the slab outside this last connected streamline will be carried down with the matrix. More importantly Figs. 4c and 5c show that this lost fluid cannot interact with the overlying mantle wedge. Therefore the melt extracted at the arc should show a smaller slab signature and material behind the arc should show no slab signature.

A more quantitative measure of this behaviour can be found by calculating the melt flux from the extraction zone and the "slab fraction" of the total flux that is derived from the subducting slab. Unfortunately, unlike the ridge model, the melt flux from the extraction region is not uniquely determined. As before, it is given by:

$$\frac{dM_T}{dt} = \rho_f \phi_0 U_0 L \left| \psi_{T \text{ bound}}^f - \psi_{T \text{ min}}^f \right| \quad (33a)$$

where:

$$\psi_{T \text{ bound}}^f = 2 \frac{w_0}{U_0} (-2D)^{1/2} \quad (33b)$$

is the value of the bounding streamline that connects the arc to the mantle and  $\psi_{T \text{ min}}^f$  is the streamline that intersects the subducting slab ( $\theta = \beta$ ) at some arbitrary distance  $r_{\text{min}}$ . As  $r_{\text{min}} \rightarrow 0$  the flux becomes unbounded. As there is no preferred minimum distance, the calculated melt flux is at best an estimate although a reasonable range of values are calculated for  $r_{\text{min}} = 2^{1/2}L/4$ . The surface through which the flux is calculated is shown in all the figures.

If  $w_0/U_0$  is greater than critical, the slab fraction is clearly 100%; however, if  $w_0/U_0$  is less than critical the slab fraction is given by:

$$S_f = \frac{|\psi_{T \text{ sad}}^f - \psi_{T \text{ min}}^f|}{|\psi_{T \text{ bound}}^f - \psi_{T \text{ min}}^f|} \quad (34)$$

where  $\psi_{T \text{ sad}}^f$  is the value of the melt stream function at the saddlepoint.

As was remarked before, the behaviour of even this simplest model for melt extraction at subduction zones is surprisingly complex and shows that many of the ad hoc assumptions of the structure of subduction zones will have to be reevaluated. Furthermore, this model can be tested quantitatively and can be used to place constraints on important parameters such as the porosity and matrix shear viscosity. The discussion will deal with these tests and their implications for the processes of melt extraction acting at subduction zones.

## 7. Discussion

Before discussing these models it is worth reviewing the assumptions made and their implications. Because of the primary assumptions of constant porosity and no melting, these models of melt extraction are not complete models of melting and segregation. They indicate how melt will flow *if it is present*, but cannot predict its distribution. When melting is included in a 2-D model, there will necessarily be porosity gradients (Appendix C) and these could lead to instabilities or other unforeseen behaviour. Nevertheless, if melting does not seriously perturb the matrix flow then the most significant feature of the simple models, extraction and concentration of melt by matrix shear, should carry through. The physical reason for this statement is clear. The focussing of melt towards the corner depends on the  $\nabla^2 V$  term in equation (4) and therefore depends only on the matrix velocity field. On the length scale of this problem, 10–100 km, mass balance indicates that the real flow of the matrix near a ridge crest or subduction zone should approximate the ideal corner flow of the simple models and one should expect the melt to move in a manner similar to that illustrated in Figs. 2–5. If this is the case, then these models offer some simple explanations

for many of the major features of the geometry of ridge and subduction related volcanism.

In the case of mid-ocean ridges, melt is extruded at the surface in narrow belts no more than 5 km wide, yet the most reasonable mechanism for melt production, adiabatic pressure release, suggests that a broad partially molten zone should exist beneath ridges to depths of  $\sim 60$  km [3]. The constant porosity ridge model reconciles both observations by permitting the extraction of small melt fractions from a large region while at the same time extruding it at the surface in a narrow band. This model is also consistent with the observation that ridges appear to be passive features uncoupled to any deep mantle structure [14]. The melt suction mechanism proposed here is strictly a local effect that depends only on the mantle deformation near a ridge crest and does not require the presence of a deep mantle plume.

As for subduction related magmatism, the most notable feature is that nearly all major volcanic arcs lie in a narrow band 100–150 km above the seismically active region of the subducting slab [15]. While it is possible that significant partial melting occurs in this depth range, an alternative explanation is afforded by the subduction zone extraction model. Figs. 4 and 5 show that, regardless of melt source, the principal fraction of melt in the mantle wedge will be drawn to the intersection of the upper plate and the subducting slab. This junction should occur at the base of the mechanical boundary layer of the upper plate at depths of 90–100 km and the seismic zone in the subducting slab should be somewhat deeper. The simple model shows that there should always be a volcanic arc above the slab junction; however it also indicates that the nature of the melts extracted can vary enormously depending on local conditions. Thus this model can qualitatively explain both the constancy of volcanic arc geometry and the variety of island arc geochemistry.

While the qualitative similarities are striking, the models can also be tested quantitatively. The most important results of these models are that they give us a length scale,  $L$ , and a velocity scale  $w_0$ , for melt extraction. With these, constraints can be placed on the two most poorly known parameters in the model, the matrix shear viscosity which controls  $L$  and the porosity which dominates  $w_0$ .

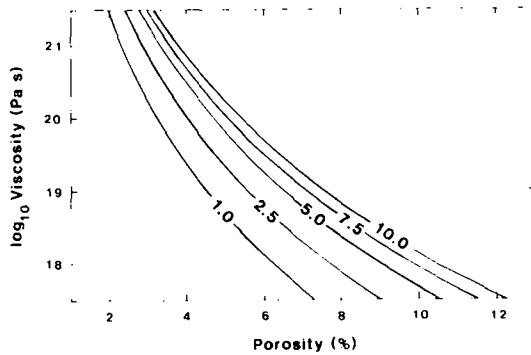


Fig. 7. Values of  $\eta$ ,  $\phi_0$ , and  $U_0$  that will produce 6 km of oceanic crust as calculated from the ridge model. Contours are half spreading rates in  $\text{cm yr}^{-1}$ .

For the ridge model, the crustal thickness produced by the extraction zone is most useful for constraining  $\eta$  and  $\phi$ . Physically, the simple model implies that the prerequisite 6 km of oceanic crust can either be produced by extracting small melt fractions from a wide area or larger melt fractions from a narrow extraction zone. Fig. 7 shows the combinations of  $\eta$  and  $\phi$  for a given half spreading rate that will produce 6 km of crust as calculated from the constant porosity model. As spreading rates are known, if limits can be placed on either viscosity or porosity, then the other parameter can be determined. Fortunately, there are at least two independent arguments for viscosity and porosity and both favor the combination of high viscosity,  $10^{20}$ – $10^{21}$  Pa s, and small porosity, 2–4%.

The simplest explanation for axial ridge valleys is that they are dynamically supported, and their width then depends on the matrix viscosity [10,11,17]. Under these conditions they should be supported by the same stresses responsible for melt extraction and therefore the length scale given by the width of axial valleys should be related to the length scale of melt extraction. Skilbeck [10]

shows that to support axial valleys tens of kilometers in width requires shear viscosities of  $10^{20}$ – $10^{21}$  Pa s. This argument is certainly valid for slow-spreading ridges that show prominent axial valleys, but is more problematic for fast spreading ridges without axial valleys.

For estimates of the mean porosity of the melting zone beneath ridges, a simple scaling argument (Appendix C) shows it must be small  $\sim$  2–4% if reasonable assumptions are made about melting and melt extraction. This argument estimates the mean porosity that can be supported by a given melting rate against compaction due to melt extraction. The results are shown in Table 2 and show two important features. First for reasonable degrees of total melt generation (10–20% by volume) the porosity at any time is small, 2–3%. This is supported quantitatively by the 1-D melting models [6,7]. Second, Table 2 implies that faster spreading ridges should have slightly higher porosities. Physically this also makes sense. If the primary melting mechanism is adiabatic pressure release [3] then the melting rate should be proportional to the upwelling velocity and faster melting rates can support higher porosities.

The implications of these two results are clear. First, if  $\phi$  is small, the simple model requires a large extraction length to produce 6 km of crust. Inspection of Fig. 7 shows that this implies a large matrix viscosity, consistent with the shape of axial valleys. Second, if the porosity increases with spreading rate it is possible to reconcile the results of the simple model with the observation that oceanic crustal thickness is apparently independent of spreading rate. Equation (27) and Fig. 7 both imply that to produce a constant 6 km of crust requires a small increase in the porosity,  $\sim$  1% for an order of magnitude increase in the spreading rate, which is comparable to the increase in porosity predicted by the simple scaling argument. This argument is self consistent and fits

TABLE 2

Expected mean porosity (%) as a function of the degree of partial melting and spreading rate

Total degree of partial melting	Half spreading rate ( $\text{cm yr}^{-1}$ )				
	1.0	2.5	5.0	7.5	10.0
10%	1.2	1.6	2.0	2.3	2.5
20%	1.6	2.1	2.6	3.0	3.3

both qualitatively and quantitatively what little is known of the melt extraction processes at mid-ocean ridges.

If little is known about melt production and extraction at ridges, even less is known about the processes governing subduction related volcanism. Fortunately, the subduction zone model is insensitive to the nature of the “melt” or “fluid” derived from the slab or to how it moves out of the slab. As long as a low viscosity phase is present at the surface of the slab, the simple model indicates how it should flow through the mantle wedge. However, if that phase can be identified by its isotopic “slab signature” and can maintain that signature throughout its movement, the simple model presented here offers several quantitative internal checks for validity. The isotopic ratio we will use for determining slab signature is  $^{87}\text{Sr}/^{86}\text{Sr}$  as it records sea water alteration of the oceanic crust by hydrothermal circulation through the ridge flanks [21]. Altered oceanic crust should show a higher  $^{87}\text{Sr}/^{86}\text{Sr}$  ratio than unaltered crust. This geochemistry forms the basis for tests of the simple model, which we will first outline and then apply to the central-eastern Aleutians and show that this model can account for the observations in a consistent manner.

The subduction zone model offers three independent methods for estimating  $L$  and  $w_0/U_0$ . The first and most obvious test gives a direct measure of the length scale of extraction. The simple model predicts that the primary arc should show signs of shallow melting with some slab signature while the first melts to reach the surface behind the arc should show signs of deeper melting or no slab signature at all. The distance behind the arc where this change should occur is roughly  $r = L_T$  and depends only on the angle of subduction and the length scale of extraction. Therefore, to find  $L$  requires a carefully sampled traverse across an arc of known subduction angle showing secondary back arc magmatism from  $\sim 3$ –100 km behind the arc. Any abrupt change in chemistry will give the length scale of extraction. If  $L$  can be determined by this method and the volume flux per length of trench is known, then constraints can be placed on  $w_0/U_0$  as was done for the ridge problem. Fig. 8 shows the melt-flux/ $L_T$  plotted against subduction angle for contours of  $w_0/U_0$  as calculated from the simple model. If  $L_T$ , the

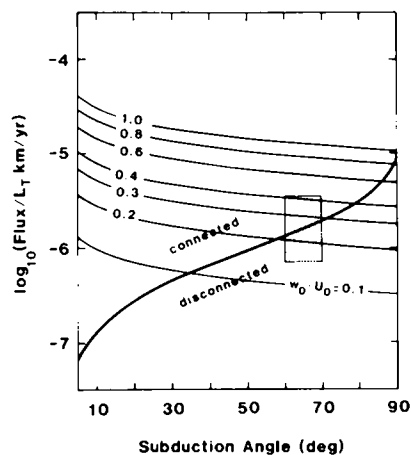


Fig. 8. Volcanic arc melt flux (per length of arc,  $\text{km}^2 \text{yr}^{-1}$ ) normalized by  $L_T$ , as a function of subduction angle and  $w_0/U_0$ . The bold line shows flux/ $L_T$  for critical values of  $w_0/U_0$ . Values plotting above the critical line have slabs that connect to the surface. Values plotting below have disconnected slabs. The stippled region shows data from the Central and Eastern Aleutians and indicates that the Aleutians are near critical and should show little to no slab signature in the back-arc region.

melt flux, subduction angle and subduction rate are known then  $w_0/U_0$  can be read off the graph. The final check for consistency is geochemical. If  $\beta$  and  $w_0/U_0$  are known then Fig. 6 (or 8) predicts whether or not the slab should be connected to the back arc. If  $w_0/U_0$  is near the critical value for a given subduction angle then the back arc volcanism should show little to no slab signature.

Therefore, to test this model the following data are needed for an arc with subsidiary back arc volcanism: (1) angle of subduction near the plate junction, (2) geochemical data as a function of position behind the arc, (3) the subduction rate  $U_0$ , and (4) the flux per unit length of arc. One region where all these measurements have been carried out is the central and eastern Aleutians, especially the Cold Bay region with the second arc volcano at Amak [18]. While the geochemical data for the secondary volcanism is sparse it is still sufficient to constrain the model and explain some of the features of this region. Fig. 9 shows  $^{87}\text{Sr}/^{86}\text{Sr}$  [18] plotted against distance for the primary arc, the Frosty peak volcanoes ( $\sim 3$  km), Mount Baldy ash flow ( $\sim 10$  km), the second arc volcanoes Amak (42 km) and Bogoslof ( $\sim 50$ –60 km) and the back-arc islands of St. George (300

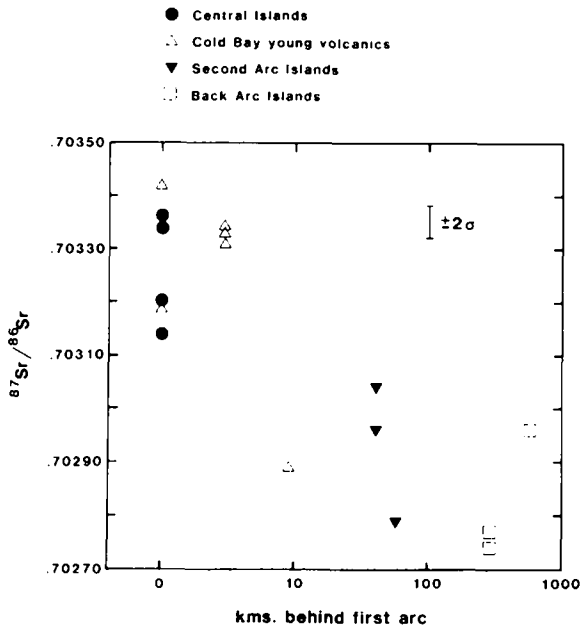


Fig. 9.  $^{87}\text{Sr}/^{86}\text{Sr}$  as a function of distance behind the primary volcanic arc for the Central and Eastern Aleutians (data from von Drach et al. [18]). Distance scale is logarithmic and data are shown for 0, 3, 9, 42, 60, 300 and 600 km. The sharp drop in  $^{87}\text{Sr}/^{86}\text{Sr}$  at  $\sim 10$  km is consistent with values at  $\sim 50$  km and behind. Far back-arc samples are for reference and should show no slab contribution.

km) and Nunivak (600 km). The last two are for reference as they should be far enough removed from the subduction zone as to only record mantle melting in the back arc region.

Fig. 9 shows a sharp drop in  $^{87}\text{Sr}/^{86}\text{Sr}$  at 10 km which is consistent with the values at 50 km and back and is representative of typical unaltered Pacific MORB levels [18]. As the subduction angle is  $\beta = 60\text{--}70^\circ$  [19] this gives a range of length scales from 10 to 50 km ( $\eta \sim 10^{20}\text{--}3 \times 10^{21}$  Pa s).

Melt flux per km of arc for the central Aleutians is calculated to be  $3.5 \times 10^{-5}$   $\text{km}^2 \text{yr}^{-1}$  [1]. Flux/ $L_T$  and  $\beta$  are plotted (Fig. 8) for the Aleutians with subduction rate 7 cm/yr [20] and give  $w_0/U_0 \sim 0.15$  for  $L_T \sim 50$  km and  $w_0/U_0 \sim 0.41$  for  $L_T \sim 10$  km. Melt streamlines for these two end members are shown in Fig. 10. For the longer length scale the slab should be entirely disconnected from the secondary arc which is consistent with the uniformly low  $^{87}\text{Sr}/^{86}\text{Sr}$  values in the back arc. For  $L_T \sim 10$  km, while the entire slab is connected, the melt streamlines for the back arc

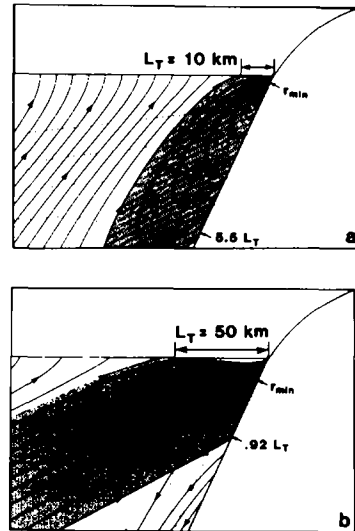


Fig. 10. Melt and matrix streamlines for the two end member models of the Aleutian arc.  $\beta = 65^\circ$ ,  $U_0 = 7$   $\text{cm yr}^{-1}$ . Length of slab sampled at the primary arc in both cases is  $\sim 50$  km. (a) Short length scale,  $L_T = \sim 10$  km ( $\eta = 1.1 \times 10^{20}$  Pa s);  $w_0/U_0 = 0.41$  ( $\phi = 1.35\%$ ), flux =  $3.2 \times 10^{-5}$   $\text{km}^2 \text{yr}^{-1}$ . (b) Long length scale,  $L_T = \sim 50$  km ( $\eta = 3.0 \times 10^{21}$  Pa s);  $w_0/U_0 = 0.14$  ( $\phi = 0.8\%$ ), flux =  $3.4 \times 10^{-5}$   $\text{km}^2 \text{yr}^{-1}$ , slab fraction = 59%.

region are probably sufficiently indirect that the slab contribution is minimal. While clearly observations from other arcs are required to say anything conclusive, this first simple test shows no glaring inconsistencies.

## 8. Conclusions

These models indicate that for reasonable matrix viscosities,  $10^{20}\text{--}10^{21}$  Pa s, the movement of melt beneath mid-ocean ridges and island arcs is controlled by non-zero  $\nabla^2 V$  shear in the matrix. The pressure gradients generated by corner flow of the matrix at spreading centers cause melt to migrate toward the ridge axis enabling the extraction of small melt fractions from a wide melting zone yet producing a narrow zone of volcanism at the surface. Similarly corner flow in the mantle wedge beneath island arcs causes melt to flow to the slab-plate junction and can account for the concentration of volcanism in regions where earthquakes in the subducting slab reach a depth of 100–150 km. The subduction zone model also implies that the geochemistry of island arc

volcanism will be strongly influenced by the geometry of melt streamlines and the connectivity of the slab with the overlying mantle wedge.

### Acknowledgements

Many thanks go to R.H. Hunter for useful advice and to G. Wasserburg for the Aleutian data. M.W. Spiegelman is supported by a Marshall Scholarship. This research forms part of a general investigation of mantle melting supported by NERC.

### Appendix A—General equations in two dimensions

The simplest set of equations for the conservation of mass and momentum in two dimensions plus time are easily derived from the general equations (1) to (5). If  $\rho_f$  and  $\rho_s$  are constant, equation (2) becomes:

$$\frac{D_v \phi}{Dt} = \frac{\partial \phi}{\partial t} + \mathbf{V} \cdot \nabla \phi = (1 - \phi) \nabla \cdot \mathbf{V} + \frac{\Gamma}{\rho_s} \quad (\text{A1})$$

Taking the curl of equation (4) gives:

$$\eta \nabla^2 (\nabla \times \mathbf{V}) = -\Delta \rho g \frac{\partial \phi}{\partial x} = \frac{\partial \bar{p}}{\partial x} g \quad (\text{A2})$$

and adding equations (1) and (2) and substituting in (3) and (4) yields:

$$\nabla \cdot \left[ \frac{k_\phi}{\mu} (\eta \nabla^2 \mathbf{V} + (\zeta + \eta/3) \nabla (\nabla \cdot \mathbf{V}) + (1 - \phi) \Delta \rho g \hat{k}) \right] = \nabla \cdot \mathbf{V} - \frac{\Gamma \Delta \rho}{\rho_f \rho_s} \quad (\text{A3})$$

Equation (A1) is the conservation of mass for the matrix and states that the change in porosity in a frame fixed to the matrix is the difference between compaction ( $\text{Div } \mathbf{V} < 0$ ) and melting. (A2) shows that the vorticity of the matrix is maintained by horizontal porosity gradients and in general by horizontal density gradients. Equation (A3) is the most complicated of the three but the physics is quite straightforward. The left-hand side is simply the net melt flux through a small volume of matrix and the right-hand side is the sum of compaction and the volume change on melting. Therefore, the amount of melt that can be extracted from a small volume depends on how much is squeezed out by compaction and how much is expelled by the increased volume of the melt. Preliminary work indicates that (A3) will be dominated by the non-linear behaviour of the permeability with respect to small changes in porosity. Furthermore, if the volume changes are relatively small and the buoyancy term is large (third term on left-hand side of (A3)) then the compaction will be controlled by the extraction of melt by gravity and less by the viscosity of the matrix.

If the permeability and the melting function are known (or presupposed) then (A1) to (A3) can be solved for porosity and the two components of  $\mathbf{V}$ , subject to appropriate boundary

conditions. Once these are known,  $\nabla \mathcal{P}$ ,  $k_\phi$ , and therefore  $\mathbf{v}$  are completely determined by equations (3) to (5).

### Equations with constant porosity and no melting

If  $\phi = \phi_0$  and  $\Gamma = 0$ , equations (A1) to (A3) reduce to a very simple form. Equations (A1) and (A2) become, respectively:

$$\nabla \cdot \mathbf{V} = 0 \quad (\text{A4})$$

$$\nabla^2 (\nabla \times \mathbf{V}) = 0 \quad (\text{A5})$$

and (A3) vanishes identically. By writing  $\mathbf{V}$  in potential form (equation (7)) then (A4) is satisfied explicitly and (A5) reduces to the biharmonic equation which is easily solved for corner flow boundary conditions.

### Appendix B—Analysis: ridge and trench models

#### Ridge model

*Estimation of wedge angle  $\alpha$ .* A straightforward definition of  $\alpha$  is shown in Fig. 1b and derives from an argument from Skilbeck [10]. If we assume that the actual shape of the lithospheric plate near a ridge axis is controlled by the thermal history of the plate then a reasonable approximation for the wedge angle is:

$$\alpha = \tan^{-1} \left[ \frac{d(L_R)}{L_R} \right] \quad (\text{B1a})$$

where

$$d(L_R) \sim 2 \left( \frac{\pi \kappa L_R}{U_0} \right)^{1/2} \quad (\text{B1b})$$

is approximately the depth a cooling pulse in an infinite half space would have traveled in time  $t = L_R/U_0$ , and therefore is approximately the thickness of the lithosphere at a distance  $L_R$  from the ridge axis.  $\kappa$  is the thermal diffusivity of the mantle and  $L_R$  is the characteristic length scale for the ridge. Unfortunately, inspection of Figs. 2 and 3 shows quite clearly that the characteristic length scale for melt extraction at ridges is:

$$L_R = L(2B)^{1/2} \quad (\text{B2})$$

where  $L$  and  $B$  are defined as before and  $B$  depends on the wedge angle  $\alpha$ . Therefore, (B2) yields a transcendental equation for  $\alpha$  which was solved using a simple iterative scheme starting from  $\alpha = 0$  in (B2).

*Solution for the bounding streamline.* Saddlepoints exist at values of  $r$  and  $\theta$  for which:

$$\mathbf{v} = \nabla \times (\psi_R \hat{j}) = \mathbf{0} \quad (\text{B3a})$$

or:

$$\frac{-w_0}{U_0} \left[ \frac{2B}{r^2} + 1 \right] \cos \theta + A \cos \theta - B(\cos \theta - \theta \sin \theta) = 0 \quad (\text{B3b})$$

$$\frac{w_0}{U_0} \left[ \frac{2B}{r^2} - 1 \right] \sin \theta + A \sin \theta - B \theta \cos \theta = 0 \quad (\text{B3c})$$

Eliminating  $r^2$  terms, saddlepoints exist where

$$g_R(\theta) = B\theta \cos 2\theta + \left( \frac{w_0}{U_0} + \frac{B}{2} - A \right) \sin 2\theta = 0 \quad (\text{B4})$$

If  $g_R(\pi/2 - \alpha) > 0$  no saddlepoints exist within the boundaries. In this case the bounding streamline is the one that is tangent to the boundaries at  $\theta = \pi/2 - \alpha$  or:

$$v_\theta(r, \pi/2 - \alpha) = \left. \frac{-\partial \psi_R^f}{\partial r} \right|_{\theta = \pi/2 - \alpha} = 0 \quad (\text{B5a})$$

that is:

$$r_{\text{tan}} = \left[ \frac{2(w_0/U_0)B}{B(\pi/2 - \alpha) \sin \alpha + \left( \frac{w_0}{U_0} - A \right) \cos \alpha} \right]^{1/2} \quad (\text{B5b})$$

#### Subduction zone model

*Critical value of  $w_0/U_0$ .* A given streamline is found by plotting:

$$a(\theta)r^2 - \psi_T^f r - 2 \frac{w_0}{U_0} (C \sin \theta + D \theta \cos \theta) = 0 \quad (\text{B6a})$$

for a fixed value of  $\psi_T^f$  where:

$$a(\theta) = C(\sin \theta - \theta \cos \theta) + D\theta \sin \theta + \frac{w_0}{U_0} \cos \theta \quad (\text{B6b})$$

Whether or not the slab is wholly connected to the wedge corner depends only on the zeros of  $a(\theta)$ . For  $\psi = 0$ , where  $a = 0$ ,  $r \rightarrow \infty$ . If  $w_0/U_0$  is greater than the critical value then  $a$  has no zeros. If  $w_0/U_0$  is less than critical,  $a$  has two zeros and the zero streamline can never connect. The critical value of  $w_0/U_0$  occurs when  $a$  has only one zero. When this happens, the zero streamline is connected but only as  $r \rightarrow \infty$ . Therefore, the critical value of  $w_0/U_0$  as a function of the subduction angle  $\beta$  can be found by solving the simultaneous equations:

$$\begin{aligned} a(\theta) &= 0 \\ da/d\theta &= 0 \end{aligned} \quad (\text{B7})$$

This was done numerically and the results are shown in Fig. 6.

*Solution for the bounding streamline.* Inspection of Figs. 4 and 5 shows that the bounding streamline that connects the mantle wedge to the wedge corner is the one that is tangent at the upper boundary ( $\theta = 0$ ). As in the ridge model, this implies that  $v_\theta = 0$  at  $\theta = 0$ . The tangent point is then easily computed to be:

$$L_T = L(-2D)^{1/2} \quad (D < 0) \quad (\text{B8})$$

and is independent of  $w_0/U_0$ . The value of the bounding streamline is then simply

$$\psi_T^f \text{ bound} = 2 \frac{w_0}{U_0} (-2D)^{1/2} \quad (\text{B9})$$

and the intersection of this streamline with the lower slab can

then be found using (B6) and (B9) with  $\theta = \beta$ . This gives:

$$r_\beta = L \left[ \frac{(-2D)^{1/2} + [2 \cos \beta (C \sin \beta + D \cos \beta) - 2D]^{1/2}}{\cos \beta} \right] \quad (\text{B10})$$

which is also independent of  $w_0/U_0$ .

*Solution of saddlepoint: subduction zone model.* In the subduction zone model the melt stream function will develop a saddlepoint if  $w_0/U_0$  is less than the critical value. As before the saddlepoint exists where  $\mathbf{v} = \nabla \times (\psi_T^f \hat{j}) = \mathbf{0}$  or solving for  $\theta$  only, the saddlepoint exists where:

$$g_T(\theta) = \frac{d}{d\theta} [(C \sin \theta + D \cos \theta) a(\theta)] = 0 \quad (\text{B11})$$

The last streamline to connect the subducting slab to the wedge corner is the streamline that passes through the saddlepoint. The point where this streamline intersects the subducting slab at  $\theta = \beta$  is solved for numerically.

## Appendix C — A scaling argument to estimate porosity in the presence of melting

In steady state, the porosity is governed by:

$$\mathbf{V} \cdot \nabla \phi = (1 - \phi) \nabla \cdot \mathbf{V} + \frac{\Gamma}{\rho_s} \quad (\text{C1})$$

which states that the equilibrium value of the porosity is controlled by the balance of compaction and melting. Now, if the results of the 1-D models are applicable to two dimensions, then compaction is primarily the result of melt extraction by differential buoyancy and equation (A3) can be approximated by:

$$\nabla \cdot \mathbf{V} \sim -\nabla \cdot \left[ \frac{k_\phi}{\mu} (1 - \phi) \Delta \rho g \hat{k} \right] + \Gamma \Delta v \quad (\text{C2})$$

where  $\Delta v$  is the volume change on melting and  $\hat{k}$  now points upwards. Equation (C2) shows that where the porosity is near zero, and therefore separation is negligible, the matrix must expand to take up the volume increase on melting. Beneath ridges, this region will be near the lower boundary of the melting zone. In this region the porosity will grow rapidly until the permeability is high enough to permit separation by buoyancy. Once separation becomes significant, however, the matrix must compact and porosity will grow more slowly. This is supported by the 1-D melting models [6,7]. Schematically this is shown in Fig. 11. An important consequence of equations (C1) and (C2) is that the porosity can never be independent of position in steady state unless  $\Gamma = 0$ .

More importantly, these equations can be used to estimate the melting rate required to support a mean porosity  $\phi_0$  against compaction, or conversely, they can be used to estimate the characteristic porosity produced by a constant rate of melting over a melting depth  $l$ . This estimate is based on the following assumptions:

- (1)  $\Gamma = \Gamma_0$  over the melting range
- (2)  $\phi \sim \phi(z)$  porosity changes are primarily in the  $z$  direc-

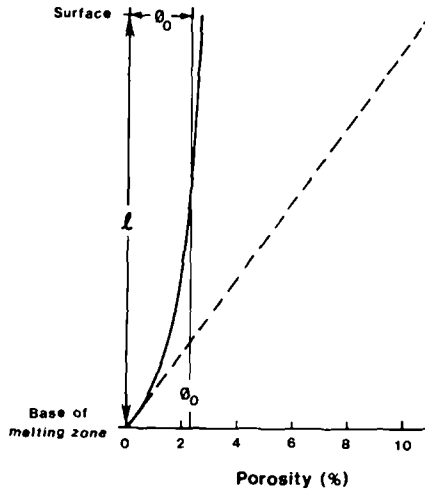


Fig. 11. Schematic diagram for scaling argument (Appendix C) showing 1-D porosity profile as a function of height above the base of the melting zone. Dashed line shows porosity profile for constant melting rate and no separation. Solid curve is the porosity profile when separation of melt from the matrix by buoyancy is significant (see [6,7]).  $\phi_0$  is the characteristic porosity with separation.  $l$  is the thickness of the melting zone.

tion.

(3)  $(1 - \phi) \sim 1$  mean porosity is small

(4)  $k_\phi \sim a^2 \phi^n / c$

(5)  $\Delta v$  is negligible

Substituting these into (C1) and (C2) yields:

$$\frac{\partial \phi}{\partial z} \left( W + \frac{nk_\phi}{\phi\mu} \Delta \rho g \right) \sim \frac{\Gamma_0}{\rho_s} \quad (C3)$$

Now,  $W \sim U_0$  and inspection of Figure 11 shows that:

$$\phi \sim \phi_0 \quad (C4)$$

where  $\phi_0$  is the characteristic porosity. To first order then, (C3) becomes:

$$p \sim \phi_0 \left( 1 + n \frac{w_0}{U_0} \right) \quad (C5a)$$

where:

$$p = l \Gamma_0 / \rho_s U_0 \quad (C5b)$$

is the "total degree of partial melting", that is, the volume fraction of matrix melted by passing through a constant melting zone of length  $l$  at speed  $U_0$ . Physically (C5a) is reasonable as it shows that in the absence of separation ( $w_0 = 0$ ) the porosity equals the degree of partial melting whereas if separation is important, the mean porosity must be smaller than  $p$ . (C5) also shows that for a fixed degree of partial melting, fast spreading ridges should show a slightly higher porosity. This is also reasonable as (C5b) shows that to produce the same degree of partial melting at fast ridges requires a higher

melting rate and higher melting rates can support higher mean porosities.

## References

- 1 J.A. Crisp, Rates of magma emplacement and volcanic output, *J. Volcanol.* 20, 177-211, 1984.
- 2 N.H. Sleep, Segregation of magma from a mostly crystalline mush, *Geol. Soc. Am. Bull.* 85, 1225-1232, 1974.
- 3 D. McKenzie, The generation and compaction of partially molten rock, *J. Petrol.* 25, 713-765, 1984.
- 4 D.R. Scott and D.J. Stephenson, Magma solitons, *Geophys. Res. Lett.* 11, 1161-1164, 1984.
- 5 F.M. Richter and D. McKenzie, Dynamical models for melt segregation from a deformable matrix, *J. Geol.* 92, 729-740, 1984.
- 6 N.M. Ribe, The deformation and compaction of partial molten zones, *Geophys. J.* 83, 487-501, 1985.
- 7 F.M. Richter, Simple models for trace element fractionation during melt segregation, *Earth Planet. Sci. Lett.* 77, 333-344, 1986.
- 8 D.R. Scott, D.J. Stephenson and J.A. Whitehead, Observations of solitary waves in a viscously deformable pipe, *Nature* 319, 759-761, 1986.
- 9 D. McKenzie, Speculations on consequences and causes of plate motions, *Geophys. J.* 18, 1-32, 1969.
- 10 J.N. Skilbeck, On the fluid dynamics of ridge crests, in: Notes on the 1975 Summer Study Program in Geophysical Fluid Dynamics at the Woods Hole Oceanographic Institution, Vol. 2, pp. 113-122, Woods Hole Ocean. Inst. Ref. No. 75-58, 1975.
- 11 A.H. Lachenbruch, Dynamics of a passive spreading center, *J. Geophys. Res.* 81, 1883-1902, 1976.
- 12 G.K. Batchelor, *An Introduction to Fluid Dynamics*, Cambridge University Press, 1967.
- 13 F.A.L. Dullien, *Porous Media Transport and Pore Structure*, Academic Press, New York, N.Y., 1979.
- 14 G. Houseman, The deep structure of ocean ridges in a convecting mantle, *Earth Planet. Sci. Lett.* 64, 283-294, 1983.
- 15 B.L. Isacks and M. Barazangi, Geometry of benioff zones: lateral segmentation and downwards bending of the subducted lithosphere, in: *Island Arcs, Deep Sea Trenches and Back Arc Basins*, M. Talwani and W.C. Pitman, eds., pp. 99-114, American Geophysical Union, Washington, D.C., 1977.
- 16 B. Parsons and D. McKenzie, Mantle convection and the thermal structure of plates, *J. Geophys. Res.* 83, 4485-4496, 1978.
- 17 N.H. Sleep, Sensitivity of heat flow and gravity to the mechanism of sea floor spreading, *J. Geophys. Res.* 74, 542-549, 1969.
- 18 V. von Drach, B.D. Marsh, and G.J. Wasserburg, Nd and Sr isotopes in the Aleutians: multicomponent parenthood of island-arc magmas, *Contrib. Mineral. Petrol.* 92, 13-34, 1986.
- 19 E.R. Engdahl, Seismicity and plate subduction in the central Aleutians, in: *Island Arcs, Deep Sea Trenches and Back Arc Basins*, M. Talwani and W.C. Pitman, eds., pp. 259-271, American Geophysical Union, Washington, D.C., 1977.

- 20 K.H. Jacob, K. Nakamura, and J.N. Davies, Trench volcano gap along the Alaska-Aleutian arc: facts and speculations on the role of terrigenous sediments for subduction, in: *Island Arcs, Deep Sea Trenches and Back Arc Basins*, M. Talwani and W.C. Pitman, eds., pp. 99-114. American Geophysical Union, Washington, D.C., 1977.
- 21 R.K. O'Nions, Isotopic abundances relevant to the identification of magma sources, *Philos. Trans. R. Soc. London, Ser. A* 310, 591-603, 1984.